Iranian Journal of Materials Science and Engineering, Vol. 21, Number 2, June 2024
RESEARCH PAPER

A Comparison of Microstructure, Hardness, and Wear Behavior of Ti Matrix Composites Reinforced with in-Situ Reinforcements Synthesized Using TiB_2 and B_4C

Alireza Zibanejad-Rad[1], Ali Alizadeh[1]*, Seyed Mehdi Abbasi[2]

* *alizadehh53@gmail.com*

[1] Faculty of Materials & Manufacturing Processes, Malek Ashtar University of Technology, Babaei Highway, Shabanloo Street, Tehran, Iran
[2] Metallic Materials Research Center, Malek Ashtar University of Technology, Babaei Highway, Shabanloo Street, Tehran, Iran

Received: January 2024 **Revised: April 2024** **Accepted: April 2024**
DOI: 10.22068/ijmse.3493

Abstract: *Pressureless sintering was employed at 1400°C to synthesize Ti matrix composites (TMCs) reinforced with in-situ TiB and TiC reinforcements using TiB_2 and B_4C initial reinforcements. The microstructure and wear behavior of the synthesized composites were evaluated and compared and the results showed that B4C caused the formation of TiB-TiC in-situ hybrid reinforcements in the Ti matrix. Also, TiB was in the form of blades/needles and whiskers, and TiC was almost equiaxed. Moreover, the volume fraction of the in-situ formed reinforcement using B_4C was much higher than that formed using TiB_2. In addition, although the hardness of the B_4C-synthesized composites was higher, the composite synthesized using 3 wt.% TiB_2 exhibited the highest hardness (425 HV). The wear test results showed that the sample synthesized using 3 wt.% TiB_2 showed the lowest wear rate at 50 N, mainly because of its higher hardness. The dominant wear mechanism in the samples synthesized using 3 wt.% B_4C was abrasive and delamination at 50 N and 100 N, respectively while in the samples synthesized using 3 wt.% TiB_2, a combination of delamination and adhesive wear and adhesive wear was ruling, respectively.*

Keywords: *Pressureless sintering, Titanium, Composite, Microstructure, Wear.*

1. INTRODUCTION

The incorporation of ceramic reinforcements to titanium and Ti-alloy matrices overcomes the weaknesses of these materials, such as high-temperature strength, which restricts the use of Ti and its alloys in industrial applications [1]. Hence, Ti matrix composites can be employed in various industries, including biomedicine [2], transport [3], aerospace [4], and defence [5]. Various ex-situ and in-situ reinforcements have been used to synthesize TMCs, such as carbides [6], nitrides [7], oxides [8], and hybrid ones [9]. However, the synthesis of in-situ reinforcements offers higher thermodynamic stability and enhanced matrix/reinforcement bonding, causing better physical, mechanical, and wear properties than those using ex-situ reinforcements [10, 11]. Moreover, a more homogenous distribution of the reinforcements can be achieved along with the formation of contamination-free interfaces [9]. Also, the synthesis of hybrid in-situ reinforcements could exhibits an improved strengthening effect compared with an increase in the reinforcement content [12].

There are various methods for producing Ti-matrix composites reinforced with in-situ reinforcements, such as hot isostatic pressing [13], hot pressing [14], and pressureless sintering [15]. Since pressureless sintering is capable of sintering complex shapes and is a relatively inexpensive method, it is receiving growing attention [16].

There are numerous studies on the evaluation of microstructures and mechanical properties of in-situ TMCs. For instance, Zheng et al. [17] investigated the wear behavior of Ti6Al4V alloy reinforced with various amounts of TiB+TiC using B_4C as the initial additive to form the reinforcement. They reported that by increasing the TiB+TiC content, the degree of wear decreased since the hardness increased. Sousa et al. [18] studied the tribocorrosion resistance of Ti-TiB-TiC composites obtained by reactive hot pressing under low loads such as 0.5 N. Again, they used B_4C particles to achieve the in-situ reinforcements and found that using TiB-TiC reinforcement could significantly reduce the wear volume loss owing to hardness increase. Ma et al. [19] used the reaction between B_4C and Ti-1100

[DOI: 10.22068/ijmse.3493]

alloy in a consumable vacuum furnace to create TiB+TiC reinforcement and investigated the microstructure and mechanical properties. They deduced that the composite sample exhibited enhanced tensile strength values (694.8, 669.1, and 676.4 MPa) compared with the monolithic Ti-1100 alloy (610.6, 586.2, and 556.1 MPa) owing to the strengthening effect of the reinforcement on the matrix as well as the load transfer to reinforcements. Therefore, it can be seen that almost all the papers dealing with the formation of TiB-TiC reinforcement in Ti matrices used B_4C particles. In this study, TiB_2 and B_4C particles were employed as the starting materials to form in-situ reinforcements in a pure Ti matrix. The microstructures, hardness, and wear properties obtained from TiB_2 and B_4C initial additives were compared.

2. EXPERIMENTAL PROCEDURES

To synthesize Ti/TiC+TiB composites, titanium powder was blended with 1, 2, and 3 wt.% B_4C powders in a jar mill at 80 rpm for 5 hours to obtain a homogenous powder mixture, followed by pouring the powder mixture into a mold with a diameter of 4 cm. Then, the mold was kept in a furnace for 1 hour at 250°C. Next, compressing at 550 MPa using a hydraulic press was done for 30 minutes. After cooling the mold in the furnace, cylindrical samples with dimensions of 4 cm × 4 mm were achieved.

The next step was to sinter the samples in a furnace under pure argon at 1400°C for 90 minutes with a heating rate of 10°C/min. The same process was repeated for the TiB_2 powder with the same amounts. The reason for selecting the above-mentioned parameters was to try other parameters and achieve not good enough results. For example, a sintering temperature of 1200°C did not result in the completion of reactions that caused in-situ reinforcements.

The micrographs of the as-received Ti, B_4C, and TiB_2 can be found in Fig. 1.

Scanning electron microscopy (SEM-Vega//Tescan) equipped with an energy dispersive spectroscopy (EDS) detector was employed to evaluate the as-prepared samples. The surface of the samples was ground using SiC papers. Then, alumina particles (particle size ~ 3 μm) were used to polish the samples, followed by etching in Kroll's reagent (5 ml HF + 10 ml HNO_3 + 85 ml distilled water). The holding time in the reagent solution was 10-30 seconds.

The micro-hardness measurements were done using a Vickers indenter by applying a 30 kgf load with a dwell time of 20 s. The data reported was the average of at least five measurements according to the ASTM E92-82 standard. Porosity measurements were carried out using the following formula [20]:

$$P = 1 - \frac{\rho_{ac}}{\rho_{th}}$$

where ρ_{ac} is the actual density of the samples measured by Archimedes' principle [21] and ρ_{th} is the theoretical density calculated by the rule of mixtures.

Dry wear tests (pin-on-disc mode) were conducted at room temperature, a sliding distance of 1000 m, a sliding velocity of 0.6 m/s, and the applied loads of 50 N and 100 N. The ASTM standard used to perform the wear tests was the ASTM G99.

3. RESULTS AND DISCUSSION

3.1. Microstructural Observations

Figure 2 depicts the SEM micrographs of Ti/TiC+TiB composite synthesized using B_4C particles. As can be seen, almost no porosity can be found, which can be related to the high synthesis temperature chosen since at 1300°C with the same additives and process, porosity was seen in the microstructure [9].

The other noteworthy point is the formation of TiB as both needles/blades and whiskers. The formation of TiB needles/blades has been reported by some researchers [22, 23], while the formation of TiB whiskers is in agreement with the results reported by other works [24]. The formation of TiB and TiC can be proved by both the EDS analysis result in Fig. 3 and XRD patterns in Fig. 4. In addition, it could be deduced that no unreacted B_4C was present in the structure or its amount was so low that could not be detected by the XRD analysis (Fig. 4). Moreover, it can be stated that with an increase in the B_4C content (as can be seen in Fig. 2c), the amount of the whiskers formed increased, and the fibers became more aligned in one direction.

[DOI: 10.22068/ijmse.3493]

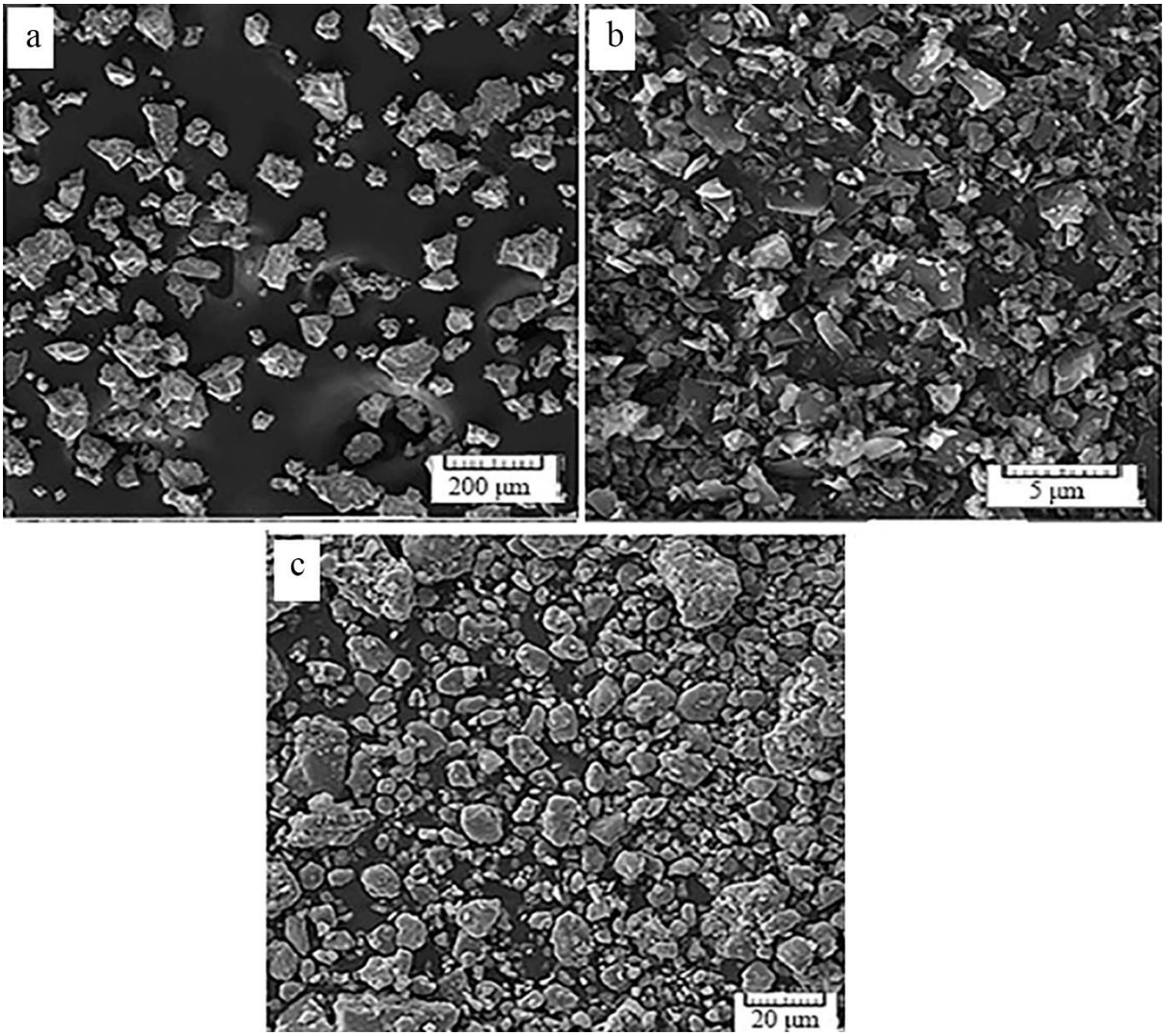

Fig. 1. Micrographs of the as-received powders: (a) Ti, (b) B_4C, (c) TiB_2.

On the other hand, TiC can be seen in the form of almost equiaxed particles with an aspect ratio of about 1. Moreover, the EDS analysis of points A and B in the SEM micrographs of Fig. 2 can be seen in Fig. 3. It can be seen that point A consisted of Ti, B, and C, while point B contained Ti and B. Therefore, it could be stated that the formation of TiB-TiC hybrid in situ reinforcement in the samples synthesized using B_4C was confirmed.

Figure 5 shows the SEM micrographs of Ti/TiC+TiB composite synthesized using TiB_2 particles. In these samples, unlike the samples fabricated using B_4C, porosity can be seen in the region of the formation of the reinforcement. The measured porosity percentages are presented in Table 1. As the results show, the porosity of the samples that were synthesized using TiB_2 particles is around 2.5 higher than their counterparts synthesized using B_4C. This can be ascribed to the higher sinterability of B_4C than that of TiB_2. According to the literature, at the same temperature, the relative density of B_4C was around 82.3% [25] while that of TiB_2 was about 67% [26].

The microstructures of Fig. 5 also show that the in-situ TiB reinforcement is in the form of whiskers/blades in most regions along with almost equiaxed particles with a lower contribution. However, when 3 wt.% TiB_2 was used, and the contribution of equiaxed TiB was more outstanding. More interestingly, this reinforcement was not integrated, but each blade/needle consisted of many pieces. Moreover, it seems that with an increase in the TiB_2 content, the orientation of TiB whiskers/blades became more random, and they became closer to each other.

[DOI: 10.22068/ijmse.3493]

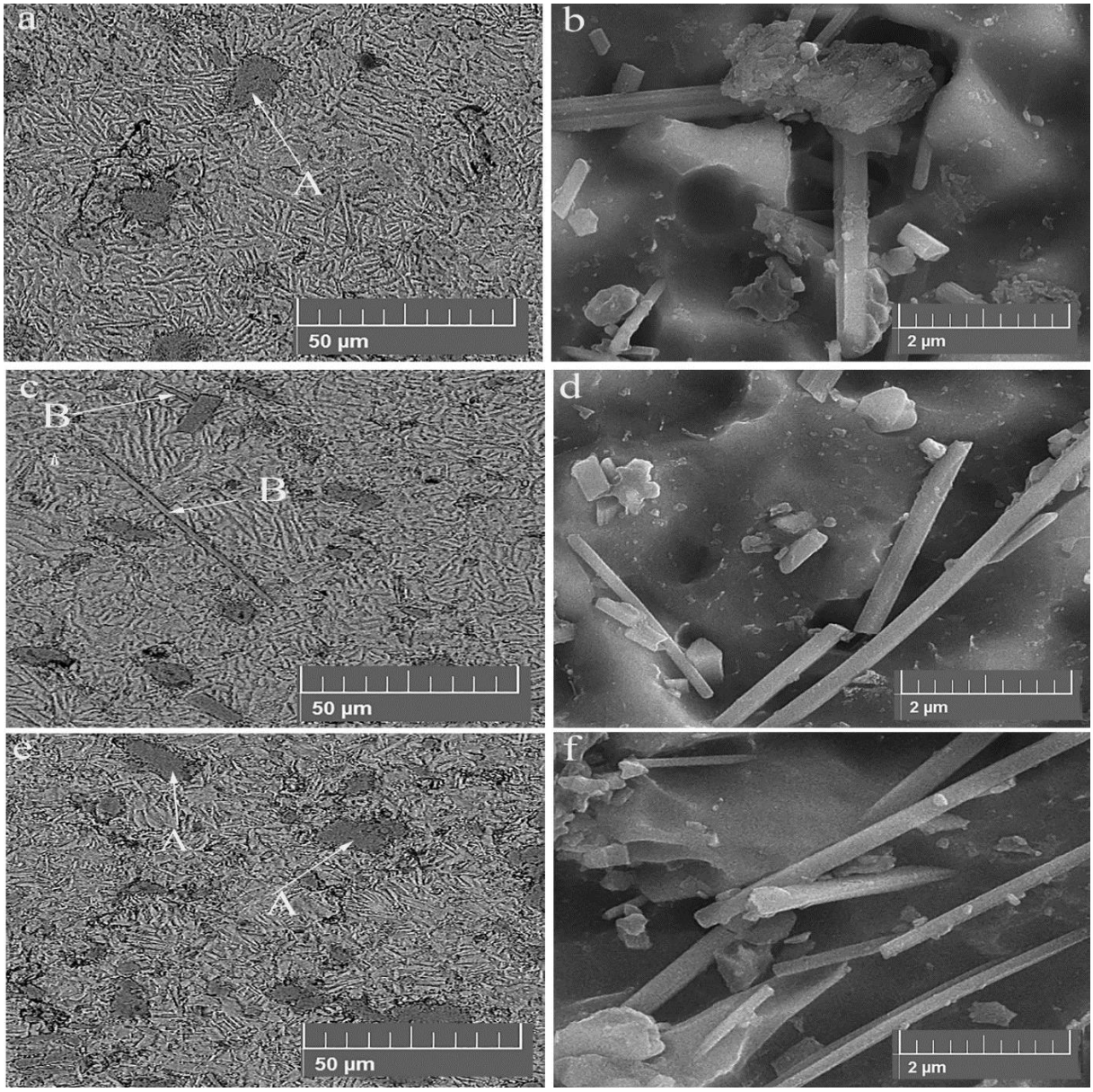

Fig. 2. SEM micrographs of the samples synthesized using B_4C: a,b) 1 wt.% B_4C, c,d) 2 wt.% B_4C. e,f) 3 wt.% B_4C

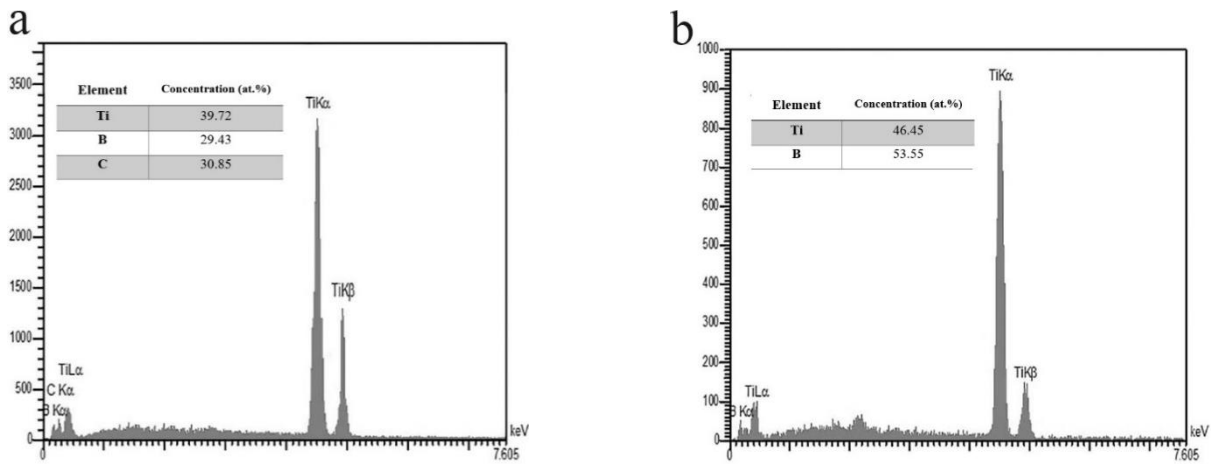

Fig. 3. EDS analysis of a) point A and b) point B in Fig. 1.

[DOI: 10.22068/ijmse.3493]

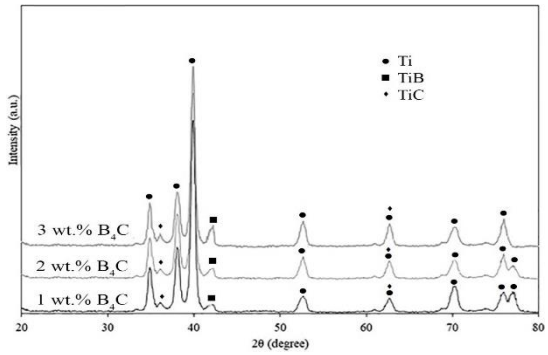

Fig. 4. XRD patterns of the samples synthesized using B_4C.

This led to the accumulation of the reinforcement in some regions and depletion of the matrix from the reinforcement in other ones, which could be another negative result. In other words, the distribution of the reinforcement was inappropriate. Also, as expected, when TiB_2 was used, the reinforcement formed was only TiB. Fig. 5f shows the SEM micrograph of the sample synthesized using 3 wt.% TiB_2. In this sample, one can see the formation of a few whiskers in the microstructure. However, if compared with Fig. 2f, the sample synthesized using 3 wt.% B_4C contained much more fibers formed mostly in one direction. This may be explained by the fact that TiB_2 is a ceramic with an anisotropic coefficient of thermal expansion (CTE), which has different values of CTE along crystallographic axes [27]. Hence, when cooled from high temperatures, the formation of whiskers can be expected but not in one direction. Therefore, it could be deduced that if the formation of TiB whiskers is favored, B_4C will be more desired at relatively high temperatures.

The other important conclusion is that a crack can be seen in one of the fibers in Fig. 5f, which shows that this sample is susceptible to cracking, while no cracks were found in the samples synthesized using B_4C particles. This can be also explained by the difference in the CTE of Ti, B_4C, and TiB_2. The CTE of Ti at 1400°C is about 4.76×10^{-5} K^{-1} [28], while that of B_4C is 2.52×10^{-6} K^{-1} [27]. On the other hand, TiB_2 has an anisotropic CTE, i.e., it has different CTEs along c and crystallographic axes, which are 7.19×10^{-6} K^{-1} and 9.72×10^{-6} K^{-1}, respectively [27]. Therefore, it can be seen that the CTE mismatch between Ti and TiB_2, in both axes, is higher than that between Ti and B_4C, leading to an increased possibility of crack formation when synthesizing using TiB_2. On the other hand, as stated by Basu et al. [27], TiB_2 with an anisotropic CTE, often develops microcracks when they are cooled from high temperatures.

In addition, the EDS analysis of point C, as an example, showed atomic percentages of 45.04 and 54.96 for boron and titanium, respectively. Therefore, the formation of TiB was confirmed. The EDS analysis of other points shown by the arrows in Fig. 5 showed similar values of Ti and B. In addition, the XRD patterns of the samples synthesized using TiB_2 in Fig. 6 confirm the absence of other phases rather than TiB.

Figure 7 displays the variations of the size and amount of the in-situ reinforcements formed with the different additives used at 1400°C measured using the ImageJ software. As can be seen, the volume fraction of the in-situ reinforcement formed using B_4C was much higher than that formed using TiB_2 so the volume fractions were 5.5, 9.2, and 15.7 % for using 1, 2, and 3 wt.% B_4C, respectively, while the volume fractions were 1.5, 2.6, and 4.0% for using 1, 2, and 3 wt.% TiB_2, respectively. Fig. 7b shows that the amount of the in-situ reinforcements increased with an increase in the starting material in both cases. This was expected because when a higher amount of additive is available, more material enters the reaction of the formation of the in-situ reinforcement, and more amounts of the reaction product will be obtained. Comparing the results of both starting materials, it could be found that finer particles can be achieved when the TiB_2 additive was employed, while the uniformity of the particle shape decreases since most of the particles formed were of needle/blade type.

Table 1. Porosity percentages of the samples.

Additive	Weight percentage	Porosity (%)
B_4C	1	1.55
B_4C	2	1.63
B_4C	3	1.78
TiB_2	1	4.42
TiB_2	2	4.48
TiB_2	3	4.56

[DOI: 10.22068/ijmse.3493]

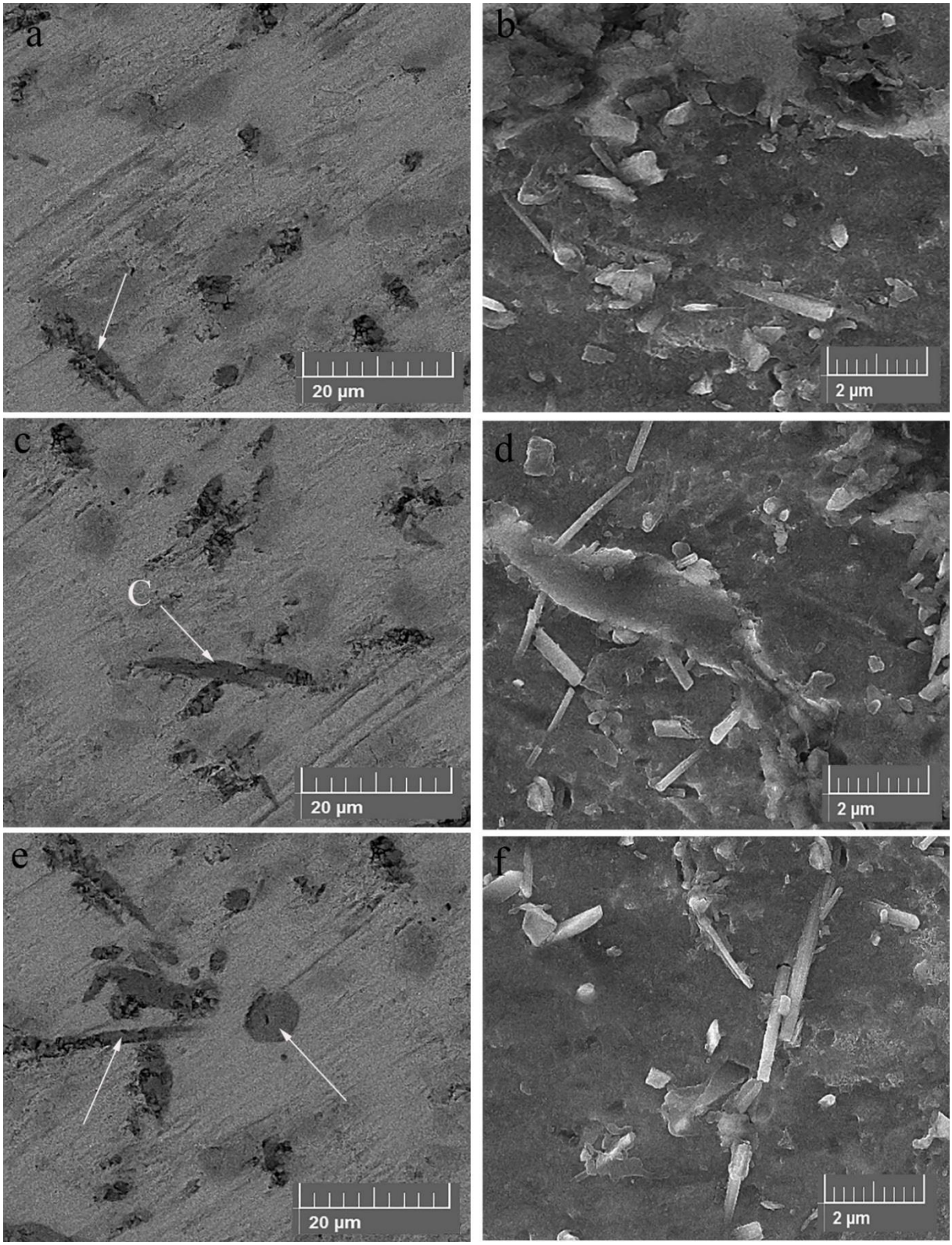

Fig. 5. SEM micrographs of the samples synthesized using TiB_2: a,b) 1 wt.% TiB_2, c,d) 2 wt.% TiB_2. e,f) 3 wt.% TiB_2.

This can be found from the standard deviation of the data in Fig. 7b. However, using B_4C, coarser particles were achieved while they were more uniform since more equiaxed particles could be

[DOI: 10.22068/ijmse.3493]

obtained in this case. The formation of finer in-situ reinforcement can be ascribed to the fragmentation of the particles formed when TiB_2 was used. As mentioned earlier, a high CTE mismatch between titanium and TiB_2 led to the propagation of cracks in the in-situ reinforcement, causing the fragmentation of these particles and a reduction in the particle size.

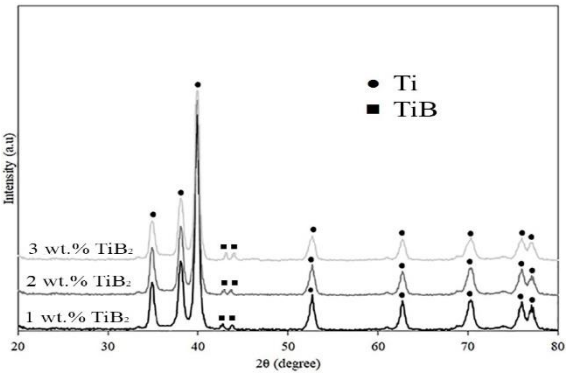

Fig. 6. XRD patterns of the samples synthesized using TiB_2.

In general, it was understood that although the use of TiB_2 led to the formation of finer in-situ reinforcement particles, B_4C could cause the creation of a hybrid reinforcement, reinforcing particles with a more uniform particle size and a higher amount of the reinforcement at the same temperature. The other important conclusion is about the distribution of the in-situ reinforcements. When using B_4C, with an increase in the B_4C content, the distribution of the in-situ reinforcement became more uniform since a higher fraction of the matrix was covered with the reinforcement, i.e., more points throughout the composite was occupied by the reinforcement (Fig. 2). However, when using TiB_2, an opposite trend was observed (Fig. 5), i.e., with an increase in the TiB_2 content, more unoccupied areas could be found in the composite and the accumulation of the synthesized reinforcement was seen.

3.2. Hardness

Figure 8 shows the variation of hardness by using various amounts of B_4C and TiB_2. It can be seen that with 1 and 2 wt.% starting materials, the hardness of the composites fabricated is relatively higher using B_4C but not to a great extent, whereas the sample synthesized using 3 wt.% B_4C exhibited a much lower hardness (378 HV) than that synthesized using 3 wt.% TiB_2 (425 HV).
Considering the volume fraction of the in-situ reinforcement in Fig. 7a, it can be understood that although using 3 wt.% TiB_2 led to a much lower content of the in-situ reinforcement than using 3 wt.% B_4C, it came with a higher hardness. This can be explained by the type and shape of the in-situ reinforcement formed in the composite. As mentioned earlier, B_4C led to the formation of TiB-TiC reinforcement while TiB_2 caused the synthesis of TiB in the composite. Bhat et al. [1] reported that the former exhibited a lower hardness (1351 HV) than the latter (1020 HV). Yi et al. [2] compared the hardness of Ti/TiB and Ti/TiB-TiC systems synthesized by the same method from two different studies and showed that the former had a higher hardness than the latter.

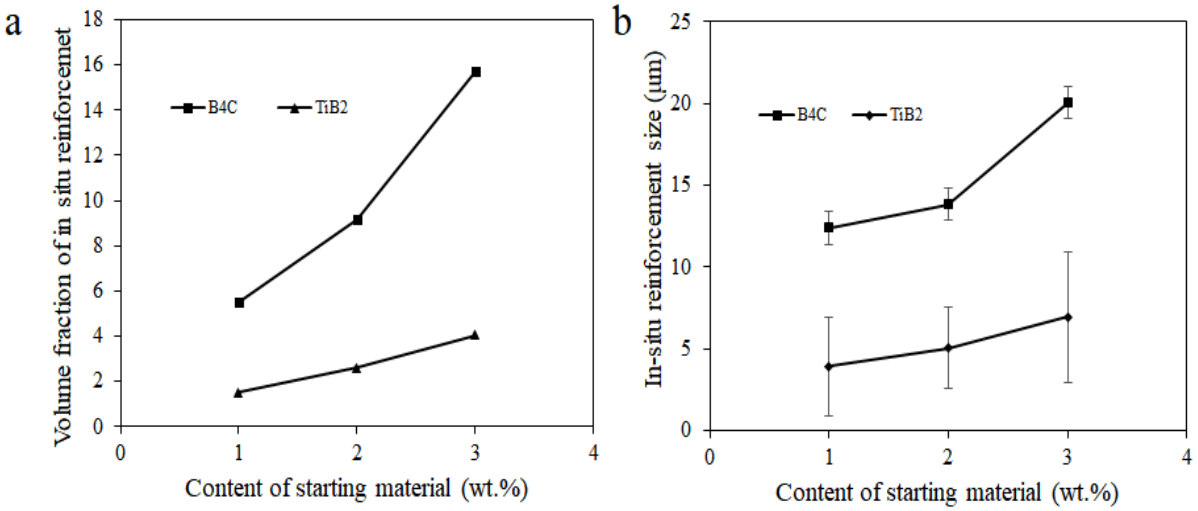

Fig. 7. Variations of a) volume fraction of the in-situ reinforcements and b) in-situ reinforcement size with the additive content.

[DOI: 10.22068/ijmse.3493]

This can be explained by the distribution of the reinforcements. In this sample, in some regions, extraordinary hardness values were achieved due to the accumulation of in-situ reinforcement while in some others, low values could be reported owing to the presence of only Ti matrix. In addition, the higher porosity percentage of the composite synthesized could contribute to a decrease in the hardness of some regions of the composite. The other reason may be the difference in morphology of the in-situ reinforcement in the two composite systems, which leads to the different toughening mechanisms, which in turn affects the mechanical properties of the material [22].

Moreover, as can be seen in Fig. 8, the error bar of the sample synthesized using 3 wt.% TiB_2 was larger than that fabricated using 3 wt.% B_4C. This can be explained by the distribution of the reinforcements. In the sample synthesized using 3 wt.% TiB_2, in some regions, extraordinary hardness values were achieved due to the accumulation of in-situ reinforcement while in some others, low values could be reported owing to the presence of only Ti matrix. In addition, the higher porosity percentage of the composite synthesized could contribute to a decrease in the hardness of some regions of the composite. However, the hardness of both Ti matrix composites using 3 wt.% TiB_2 and B_4C in this study was higher than similar composites fabricated using the spark plasma sintering process (363 HV) [29].

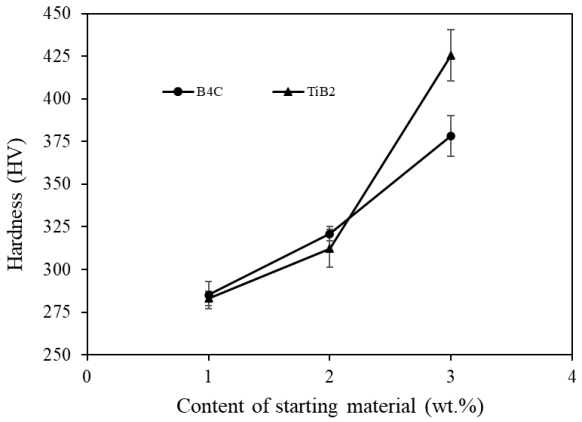

Fig. 8. Variation of hardness with the additive content.

3.3. Wear Behavior

According to Fig. 9, in both types of starting materials, the wear rate increased with an increase in the load. Also, by increasing the content of both starting materials, the wear rate decreased, which was expected because the presence of reinforcing particles increases the hardness and improves wear resistance. By increasing the amount of the reinforcing phase, the distance between the particles decreased, and the number of hard particles under contact and wear per unit length increased drastically, and as a result, the wear resistance increased [30]. According to the well-known Archard's relationship, hardness has an inverse relationship with wear rate [31]. This relationship states that with an increase in the hardness, the wear resistance increases, i.e., the wear rate decreases. Therefore, according to the hardness results in Fig. 4, it can be seen that the measured wear rates for different samples are completely consistent with this issue. In the samples synthesized using boron carbide, with an increase in the weight percentage of B_4C, the hardness increased, and the wear rate decreased. This is also true about the TiB_2 starting material. Also, if the wear rates of the composites synthesized with B_4C are compared with those synthesized using TiB_2, one can see that with 1 and 2 wt.% B_4C and TiB_2, with almost similar hardness values, almost similar wear rate values have also been obtained so that for 1 wt.% B_4C and TiB_2, the wear rate at 50 N and 100 N loads was 0.017 and 0.019 mm^3/mm, respectively, and for the composite synthesized using 1 wt.% TiB_2, the wear rate was equal to 0.018 and 0.022 mm^3/mm, respectively. Therefore, the difference between the highest and lowest wear rates was only 0.005 mm^3/mm, which is not a noticeable value. This difference between the wear rate of 2 wt.% B_4C and TiB_2 were the same. With 3 wt.% B_4C and TiB_2, the difference became even lower (0.004 mm^3/mm) due to the effect of higher amounts of starting additives. However, the lowest wear rate was not seen in the sample synthesized using B_4C at 50 N. The sample synthesized using TiB_2 showed the lowest wear rate at 50 N, mainly because of its higher hardness. However, the difference between the wear rate of this sample and that of the composite synthesized using B_4C was only 0.001 mm^3/mm. This low difference, despite the higher hardness of the TiB_2-synthesized sample, can be ascribed to both the better distribution of the in-situ reinforcements and lower porosity content in the

[DOI: 10.22068/ijmse.3493]

B_4C-synthesized sample.

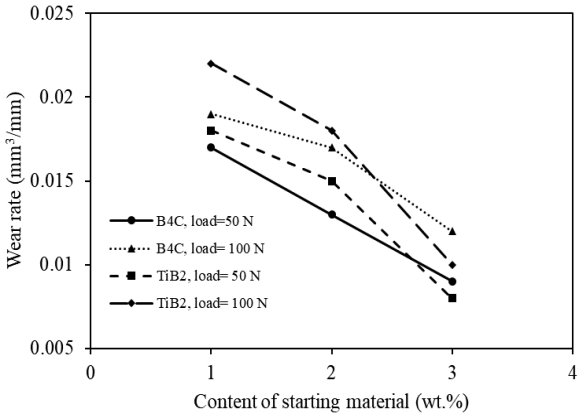

Fig. 9. Variation of the wear rate with the starting material content at the applied loads of 50 N and 100 N.

Figure 10 depicts the wear surface of the composites synthesized with 3 wt.% B_4C and TiB_2 at 50 N. The wear surface for the B_4C-synthesized sample at 1400°C shows grooves, indicating abrasive wear and also initial indications of delamination. However, no delamination occurred. Therefore, one can conclude that 50 N did not lead to any delaminations but abrasive wear was ruling. The morphology of the wear debris in this sample (Fig. 10b) shows almost no helix and layered particles, which proves that the abrasive wear mechanism was dominant in this sample.

The EDS analysis of the wear surface of this sample (Fig. 10c) also shows the presence of a significant percentage of oxygen and iron, which means the stability of the tribological layer on the wear surface. This indicates that the composite pin did not undergo severe wear, and instead of removing the material from the composite pin, the tribological layer was engaged with the steel disc. This has been reported by other studies [32, 33].

The wear surfaces of the TiB_2-synthesized sample (Fig. 10d) demonstrate indications of delamination along with grooves and plowing on the surface. Therefore, along with delamination, abrasive and adhesive wear mechanisms occurred in this sample. However, it seems that abrasive wear was not dominant but a combination of delamination and adhesive wear was dominant. The wear debris particles of this sample (Fig. 10e) were coarser than those of the B_4C-synthesized sample (Fig. 10b) with the presence of layered and helix debris, proving the occurrence of delamination and abrasive wear. The EDS analysis of the wear surface (Fig. 10f) also confirms the low amounts of oxygen and Fe, which indicates the engagement of the steel disc with the titanium matrix and the removal of Ti from the surface.

Figure 11 displays the wear surfaces of the composite samples synthesized with 3 wt.% B_4C and TiB_2 at 100 N. Unlike the wear surface of the B_4C-synthesized sample at 50 N, the wear surface of this sample at 100 N shows significant indications of delamination. In addition, grooves can be also seen on this surface, indicating the occurrence of abrasive wear. However, delamination wear was dominant in this sample. The wear debris particles of this sample were larger than that of the sample at 50 N owing to the higher applied load. The EDS analysis of the wear surface proves the existence of the tribological layer. Nonetheless, if compared with the EDS of the same sample at 50 N (Fig. 10c), it can be deduced that the oxygen and Fe percentages were lower, which can imply that the tribological layer was about to be detached and delamination would significantly remove this layer if the load continued to apply.

The wear surface of the sample synthesized with TiB_2 (Fig. 11d) shows noticeable material removal, with the dominance of adhesive wear as plowing was deeper than that occurred at 50 N. In addition, compared with the B_4C-synthesized sample at 100 N, the wear debris particles (Fig. 11e) were larger and the presence of layered helix particles is obvious owing to the occurrence of adhesive wear. The EDS analysis of the wear surface (Fig. 11f) shows high-intensity Ti peaks, which proves the loss of the tribological layer. This can be explained by the non-uniform distribution of the in-situ reinforcement in this sample, leading to the material removal in the areas without the presence of the reinforcement.

4. CONCLUSIONS

Ti matrix composites reinforced with in-situ reinforcements were fabricated by pressureless sintering using TiB_2 and B_4C at 1400°C, and the characterization and wear behavior of the composites were compared. The major conclusions of the present research are as follows:

[DOI: 10.22068/ijmse.3493]

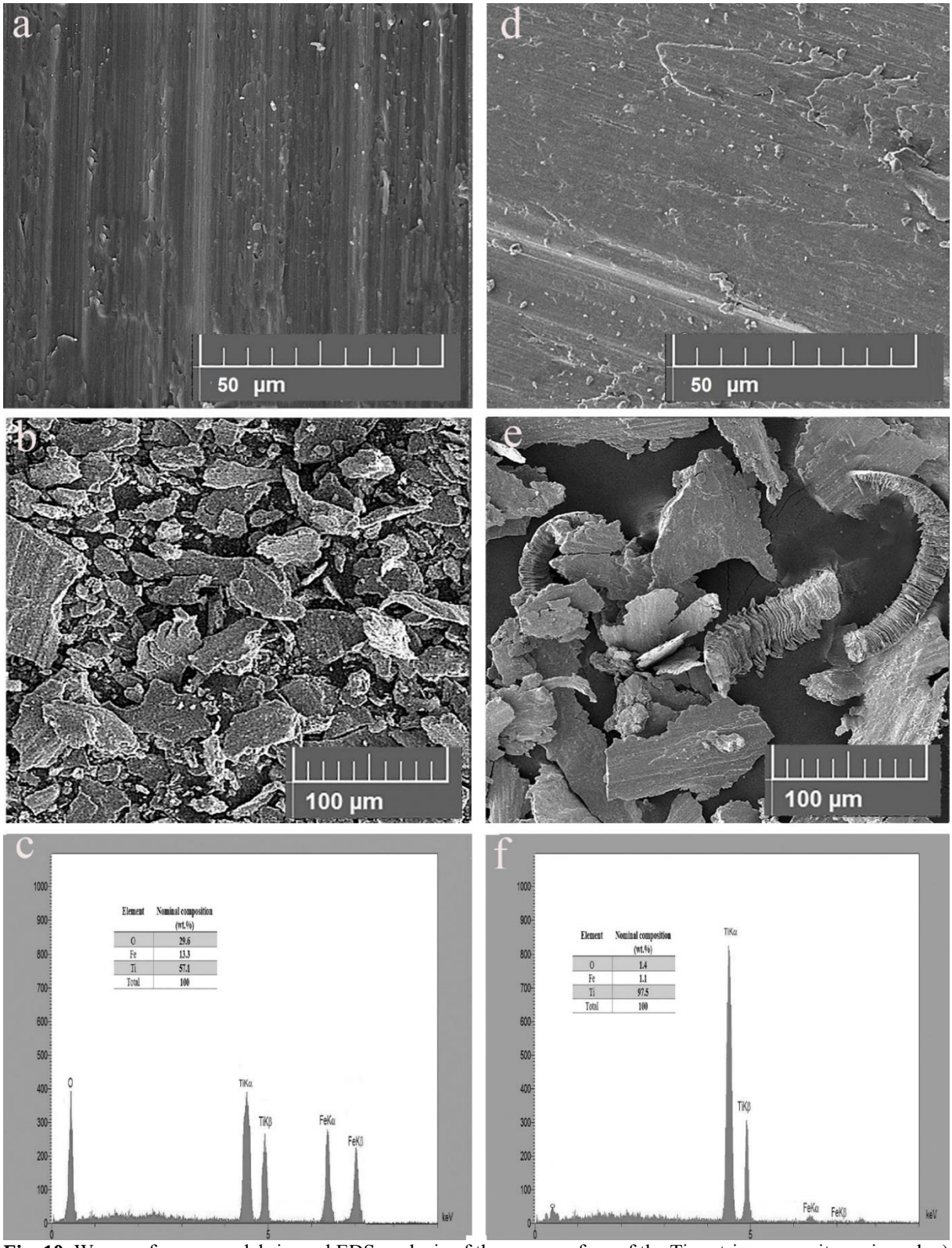

Fig. 10. Wear surface, wear debris, and EDS analysis of the Ti matrix composites using a,b,c) 3 wt.% B_4C, d,e,f) 3 wt.% TiB_2 at 50 N.

1- In the B_4C-synthesized composites, TiB-TiC in-situ hybrid reinforcement was formed while in the TiB_2-synthesized composites, TiB in situ reinforcement was formed in the

[DOI: 10.22068/ijmse.3493]

form of needles and whiskers. Moreover, the contribution of the TiB fibers was much higher in the B_4C-synthesized composites.

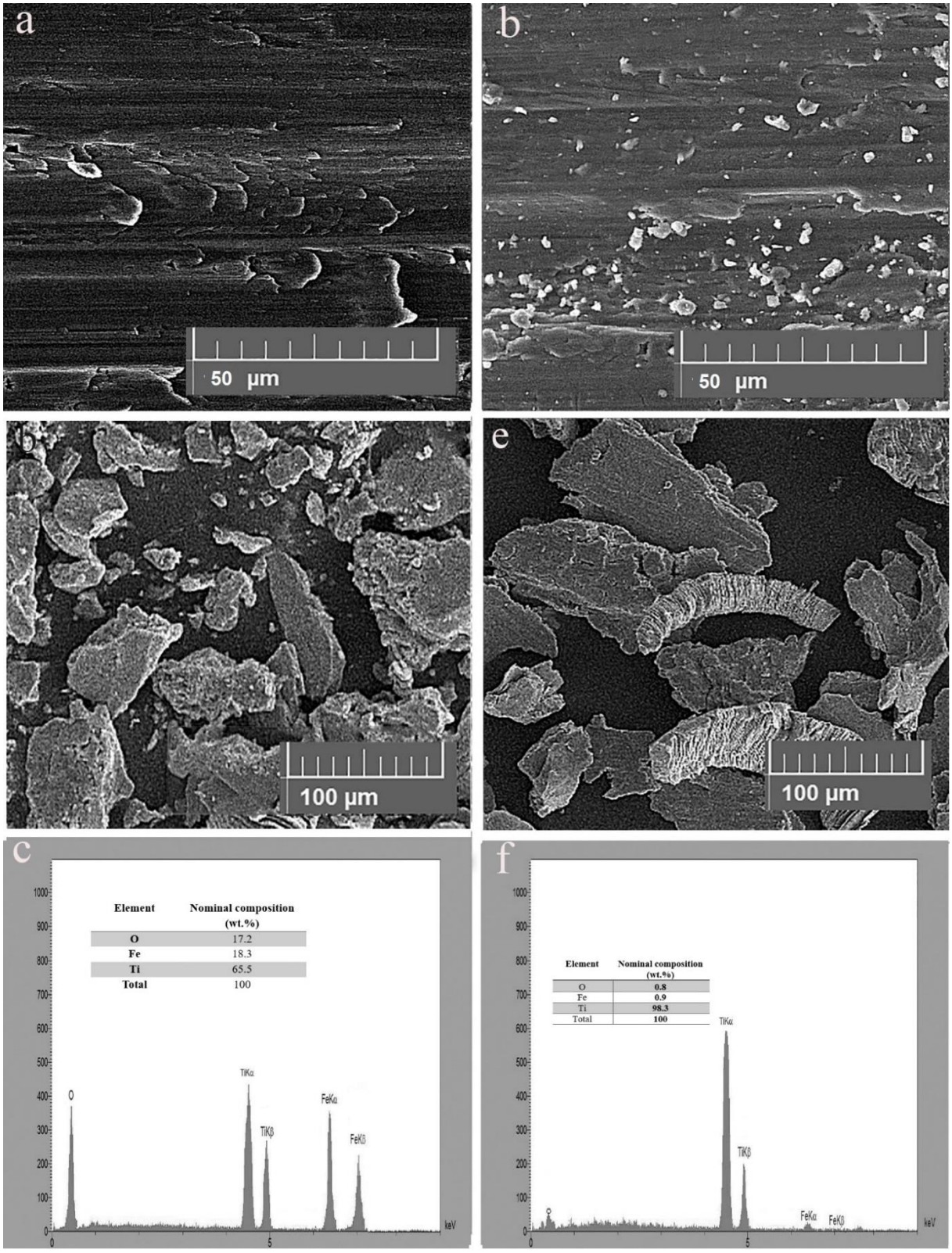

Fig. 11. Wear surface, wear debris, and EDS analysis of the wear surface of the Ti matrix composites using a, b, c) 3 wt.% B_4C, d, e, f) 3 wt.% TiB_2 at 100 N.

[DOI: 10.22068/ijmse.3493]

2- The volume fraction of the in-situ reinforcement formed using B_4C was much higher than that formed using TiB_2. However, finer reinforcements were formed in the TiB_2-synthesized composites.
3- When using B_4C, with an increase in the B_4C content, the distribution of the in-situ reinforcement became more uniform but when using TiB_2, an opposite trend was observed.
4- With 1 and 2 wt.% starting materials, the hardness of the B_4C-synthesized composites was higher, whereas the sample synthesized using 3 wt.% B_4C exhibited a much lower hardness (378 HV) than that synthesized using 3 wt.% TiB_2 (425 HV).
5- The sample was synthesized using 3 wt.% TiB_2 showed the lowest wear rate at 50 N, mainly because of its higher hardness but the difference between the wear rate of the sample and that of the composite synthesized using B_4C was only 0.001 mm^3/mm mainly due to both the better distribution of the in-situ reinforcements and lower porosity content in the B_4C-synthesized sample.
6- At 50 N, the ruling wear mechanism in the 3 wt.% B_4C-synthesized sample was abrasive with the stability of the tribological layer on the wear surface. In the 3 wt.% TiB_2-synthesized sample, a combination of delamination and adhesive wear was dominant with the loss of the tribological layer leading to the engagement of Ti with the steel disc.
7- At 100 N, delamination was dominant in the 3 wt.% B_4C-synthesized sample with the beginning of the removal of the tribological layer. In the 3 wt.% TiB_2-synthesized sample, adhesive wear with the loss of the tribological layer was ruling.

REFERENCES

[1]. Wang, X., Li, S., Han, Y., Huang, G., Mao, J., and Lu, W., "*Visual assessment of special rod-like α-Ti precipitates within the in situ TiC crystals and the mechanical responses of titanium matrix composites." Compos. B Eng.*, 2022, *230*, 109511.

[2]. Attar, H., Ehtemam-Haghighi, S., Soro, N., Kent, D., and Dargusch, M. S., "Additive manufacturing of low-cost porous titanium-based composites for biomedical applications: Advantages, challenges and opinion for future development." *J. Alloys Compd.*, 2020, *827*, 154263.

[3]. Binner, J., Porter, M., Baker, B., Zou, J., Venkatachalam, V.; Diaz, V. R., D'Angio, A., Ramanujam, P., Zhang, T., and Murthy, T., "Selection, processing, properties and applications of ultra-high temperature ceramic matrix composites, UHTCMCs–a review." *Int. Mater. Rev.*, 2020, *65* (7), 389-444.

[4]. Fereiduni, E., Ghasemi, A., and Elbestawi, M., "Selective laser melting of aluminum and titanium matrix composites: recent progress and potential applications in the aerospace industry." *Aerospace* 2020, *7* (6), 77.

[5]. Srinivasan, V., Kunjiappan, S., and Palanisamy, P. "A brief review of carbon nanotube reinforced metal matrix composites for aerospace and defence applications." *Int. Nano Lett.* 2021, 11, 321-345.

[6]. Pan, Y., Li, W., Lu, X., Hayat, M. D., Yin, L., Song, W., Qu, X., and Cao, P. "Microstructure and tribological properties of titanium matrix composites reinforced with in situ synthesized TiC particles." *Mater. Charact.* 2020, *170*, 110633.

[7]. Zhu, L., Zhang, K., Fan, S., and Wei, W., "Ti6Al4V matrix composites fabricated by laser powder bed fusion in dilute nitrogen." *Mater. Sci. Technol.* 2022, *38* (4), 207-214.

[8]. De, D., Nandi, T., and Bandyopadhyay, A., "Machining Characteristics Study of Ti-Al_2O_3 (20 Vol.% of Ti Added as Alumina Fiber into Titanium Matrix) Composite Material While Undergoing WEDM Operation. *Proceedings of I-4AM 2022*, Springer, 2022, 185-194.

[9]. Zibanejad-Rad, A., Alizadeh, A., and Abbasi, S. M. "Effect of Addition of B_4C on Microstructure and Mechanical Properties of Ti Matrix Composite Reinforced with In situ Hybrid TiB + TiC Reinforcements Fabricated by Pressureless Sintering." *T. Indian I. Metals*, 2023, 76, 1761-1770.

[10]. Zhang, X., Yu, W., Wang, J., Wang, P., Liu, Z., He, M., and Yang, Z., "Rapid in-situ synthesis, microstructure and mechanical properties of titanium matrix composites with micro/nano-sized

[DOI: 10.22068/ijmse.3493]

TiB/TiC hybrid structures." *Vacuum*, 2023, *207*, 111635.

[11]. Gao, T., Li, Z., Hu, K., Bian, Y., and Liu, X. "Assessment of AlN/Mg–8Al Composites Reinforced with In Situ and/or Ex Situ AlN Particles." *Materials* 2020, *14* (1), 52.

[12]. Yi, X., Wang, H., Sun, K., Shen, G., Meng, X., Gao, Z., and Cai, W. "Tailoring martensitic transformation and mechanical properties of Ti–Ni composite reinforced by network structure of in-situ TiB and La_2O_3 phase." *Vacuum*, 2021, *184*, 109894.

[13]. Cai, C., He, S., Li, L., Teng, Q., Song, B., Yan, C., Wei, Q., and Shi, Y., "In-situ TiB/Ti-6Al-4V composites with a tailored architecture produced by hot isostatic pressing: Microstructure evolution, enhanced tensile properties and strengthening mechanisms." *Compos. B Eng*., 2019, *164*, 546-558.

[14]. Li, S., Wang, X., Le, J., Han, Y., Zong, N., Wei, Z., Huang, G., and Lu, W., "Towards high strengthening efficiency by in-situ planting nano-TiB networks into titanium matrix composites." *Compos. B Eng.*, 2022, *245*, 110169.

[15]. Chen, T., Cai, W., Liu, Z., Ma, H., Qu, S., Zhang, W., and Yang, "C. In-situ dual-deoxidation design of advanced titanium matrix composites by pressureless sintering." *Compos. B Eng.* 2022, *244*, 110202.

[16]. Lukianova, O., Parkhomenko, A., Krasilnikov, V., Khmara, A., and Kuzmenko, A. "New method of free silicon determination in pressureless sintered silicon nitride by Raman spectroscopy and XRD." *Ceram. Int.*, 2019, 45 (11), 14338-14346.

[17]. Zheng, B., Dong, F., Yuan, X., Huang, H., Zhang, Y., Zuo, X., Luo, L., Wang, L., Su, Y., and Li, W., "Microstructure and tribological behavior of in situ synthesized (TiB+TiC)/Ti6Al4V (TiB/TiC=1/1) composites." *Tribol. Int.*, 2020, *145*, 106177.

[18]. Sousa, L., Alves, A. C., Costa, N., Gemini-Piperni, S., Rossi, A. L., Ribeiro, A. R., Simões, S., and Toptan, F., "Preliminary tribo-electrochemical and biological responses of the Ti-TiB-TiCx in-situ composites intended for load-bearing biomedical implants. *J. Alloys Compd.*, 2022, *896*, 162965.

[19]. Ma, F., Wang, T., Liu, P., Li, W., Liu, X., Chen, X., Pan, D., and Lu, W., "Mechanical properties and strengthening effects of in situ (TiB+TiC)/Ti-1100 composite at elevated temperatures." *Mater. Sci. Eng. A*, 2016, *654*, 352-358.

[20]. Zhang, P., Zhang, W., Du, Y., and Wang, Y., "High-performance Al-1.5 wt% Si-Al_2O_3 composite by vortex-free high-speed stir casting." *J. Manuf. Process.*, 2020, *56*, 1126-1135.

[21]. Arvieu, C., Galy, C., Le Guen, E., and Lacoste, E. "Relative density of SLM-produced aluminum alloy parts: Interpretation of results." *J. Manuf. Mater. Process.*, 2020, *4* (3), 83-93.

[22]. Bhat, B. R., Subramanyam, J., and Prasad, V. B., "Preparation of Ti-TiB-TiC & Ti-TiB composites by in-situ reaction hot pressing." *Mater. Sci. Eng. A*, 2002, *325* (1-2), 126-130.

[23]. Xia, M., Liu, A., Hou, Z., Li, N., Chen, Z., and Ding, H., "Microstructure growth behavior and its evolution mechanism during laser additive manufacture of in-situ reinforced (TiB+TiC)/Ti composite." *J. Alloys Compd.*, 2017, *728*, 436-444.

[24]. Gorsse, S., and Miracle, D., "Mechanical properties of Ti-6Al-4V/TiB composites with randomly oriented and aligned TiB reinforcements." *Acta Mater.*, 2003, *51* (9), 2427-2442.

[25]. Li, P., Ma, M., Wu, Y., Zhang, X., Chang, Y., Zhuge, Z., Sun, L., Hu, W., Yu, D., and Xu, B. "Preparation of dense B_4C ceramics by spark plasma sintering of high-purity nanoparticles." *J. Eur. Ceram. Soc.*, 2021, *41* (7), 3929-3936.

[26]. Zeng, L. Y., Wei, W. X., Sun, S. K., Guo, W. M., Li, H., Lin, and H. T., "Powder characteristics, sinterability, and mechanical properties of TiB2 prepared by three reduction methods." *J. Am. Ceram. Soc.*, 2019, *102* (8), 4511-4519.

[27]. Basu, B., Raju, G., and Suri, A., "Processing and properties of monolithic TiB_2 based materials. *Int. Mater. Rev.*, 2006, *51* (6), 352-374.

[28]. Paradis, P.-F., and Rhim, "W.-K. Non-

[DOI: 10.22068/ijmse.3493]

contact measurements of thermophysical properties of titanium at high temperature." *J. Chem. Thermodyn.*, 2000, *32* (1), 123-133.

[29]. Sabahi Namini, A., Azadbeh, M., and Shahedi Asl, M., "Effects of in-situ formed TiB whiskers on microstructure and mechanical properties of spark plasma sintered Ti–B_4C and Ti–TiB_2 composites." *Sci. Iran.*, 2018, *25* (2), 762-771.

[30]. Hutching, I. Tribology: Friction and Wear of Engineering Materials Science and Metallurgy. *University of Cambridge* 1992, 76-82.

[31]. Hajizamani, M., Alizadeh, M., Karamouz, M., and Alizadeh, A., "Effect of Post-Processing Annealing on Microstructure, Mechanical Behavior and Wear Characteristics of Semisolid Thermomechanically Processed Al–Zn–Mg/3 wt.% Al_2O_3 Composite." *Metallogr. Microstruct. Anal.*, 2021, *10* (3), 347-354.

[32]. Alizadeh, A.; Khayami, A., Karamouz, M., and Hajizamani, "M. Mechanical properties and wear behavior of Al5083 matrix composites reinforced with high amounts of SiC particles fabricated by combined stir casting and squeeze casting; A comparative study." *Ceram. Int.*, 2022, *48* (1), 179-189.

[33]. Alizadeh, A., Kazemi-Fard, S., and Hajizamani, M., "Microstructure, mechanical properties and wear behavior of ni-coated continuous carbon fiber-reinforced a356 aluminum matrix composites fabricated by squeeze casting." *Surf. Rev. Lett.*, 2022, *29* (12), 2250162

[DOI: 10.22068/ijmse.3493]